International Journal of Engineering Trends and Technology
ISSN: 2231–5381 / https://doi.org/10.14445/22315381/IJETT-V73I12P101

Volume 73 Issue 12, 1-9, December 2025

Original Article

Modelling Approaches for Thermal Response of RCB Under Fire Exposure

Miguel R. Manco Rivera[1], Miguel Celis Carbajal[2], Gustavo O. Guarniz Avalos[3]

[1]*Civil Engineering Department, Technological University of the Andes, Abancay, Peru.*
[2]*Mechanical Engineering Department, Federal University of Pernambuco, Recife, Brazil.*
[3]*Mechanical Engineering Department, Universidad Tecnológica del Perú, Lima, Peru.*

[1]*Corresponding Author : mmancor@utea.edu.pe*

Received: 25 June 2024 Revised: 10 December 2024 Accepted: 17 December 2024 Published: 19 December 2025

Abstract - *Reinforced Concrete Beams - RCB are widely used in buildings, bridges, and other types of infrastructure due to their versatility and high load capacity. Besides the typical service conditions, such structural systems can experience unexpected events, such as partial or total fires. Experimental tests are so expensive, and there is little data regarding these accidents. The current regulation offers some analysis options for this type of phenomenon. A localized fire generates a highly nonlinear temperature gradient that, in some cases, is capable of generating stresses in RCB structures of the same order of magnitude as their dead and live loads. These stresses are due to restrictions on thermal expansion (or contraction) and can give rise to cracking that reduces or even eliminates these stresses. Computational Fluid Dynamics (CFD) techniques provide a highly detailed description of fire-induced thermal phenomena, but their practical implementation remains limited due to computational constraints. This research proposes an integrated strategy that couples CFD-based fire analysis with Finite Element (FE) heat transfer modelling to estimate the thermal response of RCB under localized fire conditions. Additionally, this thermal field is compared with that obtained with the LF-ESF model. The analysis is performed with a unidirectional coupled model in which data derived from the CFD simulation are subsequently incorporated into the Finite Element model to determine the thermal behaviour of the system. The LF-ESF model employs updates to classical models for the temperature field distribution and heat transfer coefficients. It also employs an ellipsoidal solid flame model to describe radiative heat transfer. The results obtained are satisfactory, showing that the LF-ESF model presents conservative results, while the CFD-FEM models obtain more precise temperatures in the RCB but at a considerably higher computational cost.*

Keywords - *Localized Fire, CFD-FEM, Reinforced Concrete.*

1. Introduction

The various accidental scenarios in RC structures include seismic loads, wind loads, and thermal loads, among others. A fire implies the generation of temperature gradients that alter the thermo-mechanical response of the structure to normal operating loads [1-4]. The differences between the thermal properties of concrete and steel bars and stirrups increase the complexity of this type of analysis. The high conductivity of steel generates hotter internal zones; a non-uniform thermal gradient is not trivial to reproduce numerically. This also requires adequate refinement of the computational mesh; otherwise, the transfer of thermal information will be inaccurate.

In [5–8], different studies carried out on RCB are shown. In these studies, the thermal properties of steel and concrete are modelled as a function of temperature, allowing us to see how the behaviour varies as a function of these thermal loads. Fire scenarios consider both simple and complex models, illustrating the differences between each modelling option. In fire testing of a composite bridge [5], reinforcement bars and shear bolts in the RC slab reached maximum temperatures of less than 190 °C and 110 °C, respectively. No concrete spalling occurred, owing to the modest concrete temperatures and low slab moisture. In case [6], a trilinear compressive stress–strain model that varies with temperature is adopted for simply supported RCBs. The model's key advantage is its definition through only two parameters. Under elevated temperature conditions, the computed time–deflection curves closely matched experimental results. During fire testing of reinforced concrete beams [7], the longitudinal reinforcement was observed to improve shear performance, while the stirrups mitigated brittle vertical displacement at the onset of failure. In short RC columns [8], the concrete and steel grades have little influence on thermal failure criteria but affect the fire rating when strength criteria are considered. Therefore, various limiting failure conditions must be assessed to determine the fire resistance period. In [9–12], the

manipulation necessary for the transmission of data between FEM and CFD models is described, since normally the meshes are not coincident. The reliability of the coupling between the adiabatic surface temperature approach and the full conjugate heat transfer model is influenced by how appropriately the fire simulation results are sampled [9]. A CFD fire simulation-based study, analyzing one-way and two-way couplings on a structural system, revealed minor variations attributed to stochastic effects within the fire simulations [10]. Structural models employing shell and solid elements under fire scenarios demonstrated the capability of the method to capture global behavior and to support robust performance-based evaluations [11]. The fire behavior of a steel column was analyzed by transferring data from FDS to ANSYS through the DEVICE method and the Fire Thermomechanical Interface (FTMI). Both methods produced lateral and vertical displacements within the expected experimental error, though differences in the radial temperature distribution were noticed around peak temperature zones. These deviations result from FTMI incorporating a variable film coefficient along the thermal boundaries, while DEVICE employs a constant coefficient [12]. In [13–16], studies of steel structures subjected to various fire scenarios are addressed, as well as the transmission of data between FEM-CFD models.

The LF-ESF model described in the previous study uses updates of the classical models to describe the temperature field distribution, while the heat transfer coefficients follow the recommendations given in the Eurocode. In the calculation of radiative heat transfer, this model uses a solid ellipsoidal flame whose geometry is estimated from the HRR curve used. This flame allows the visualization factors to be updated at any time instant and allows the shadow effect between structural elements to be captured.

This work presents in a simple way the necessary steps to carry out the simulation of a localized fire in an RCB (Grade 30 MPa). Despite the relatively simple geometry of the evaluated case, the steps for the analysis of more complex structures would be the same.

2. Fire-Structure Interaction

Figure 1 shows the process of thermal energy transfer from the flame and gases toward the surfaces in contact with the fire. The overall thermal flux transferred from the fire toward the structural surface ($\boldsymbol{q''_{tot}}$ [$\mathbf{kW/m^2}$]) occurs through q''_r and q''_c, which represent radiation and convection heat fluxes and can be expressed by Equation (1):

$$q''_{tot}=q''_r+q''_c=\varepsilon_s\left[q''_{inc}-\sigma(\theta_s+273)^4\right]+h_c\left(\theta_g-\theta_s\right) \quad (1)$$

Where $q''_r = q''_{abs} - q''_{emi}$ is the net heat flux by radiation, $\boldsymbol{q''_c} = h_c(\theta_g-\theta_s)$ is the heat flux by convection, $q''_{abs}=\alpha_s q''_{inc}$ is the absorbed heat flux, q''_{inc} represents the incident heat flux, $q''_{emi}=\varepsilon_s\sigma(\theta_s+273)^4$ is the emitted heat flux, $\boldsymbol{\varepsilon_s}$ is the Non-Dimensional (ND) emissivity, $\boldsymbol{\alpha_s}$ is the ND absorptivity of the surface ($\boldsymbol{\varepsilon_s}$ and $\boldsymbol{\alpha_s}$, according to Kirchhoff's law, are equal when the surface is in thermal equilibrium with its surroundings), σ=5.67 10^{-11} [kW/m^2·K^4] is the constant of Stefan-Boltzmann and relates the total power emitted by a black body to the fourth power of its thermodynamic temperature, h_c is the coefficient of convective heat transfer and θ_s and θ_g are the surface and gas temperatures, respectively.

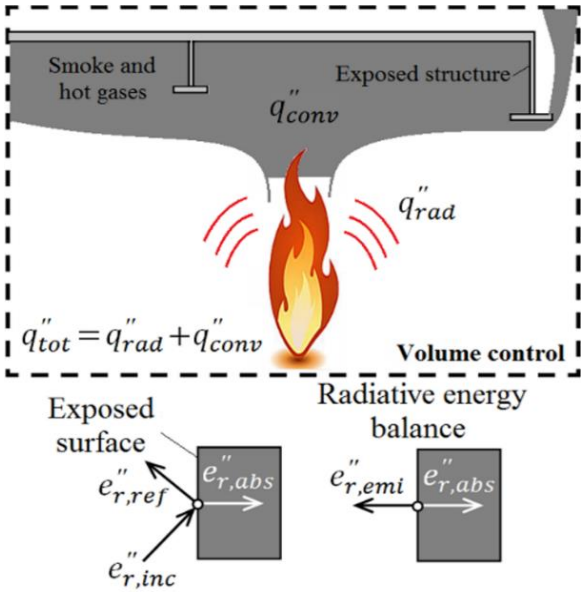

Fig. 1 Illustration of calculating the total heat flux between the fire (flame and hot gases) and the structure

The resolution of the fluid-thermo-mechanical problem, which involves simulating a fire, is addressed in three stages. Initially, the interaction between the burning process and the structure is represented through a dynamic flow model, calculating the heat fluxes on the structure's exposed surfaces. A thermal model then applies these heat fluxes to the structure to calculate temperature fields over time. Finally, the thermo-mechanical model applies this thermal field as an additional load to the previously applied operational ones. When this analysis is carried out for each time step, that is, the fire is simulated, the thermal field is calculated, and the mechanical loads are obtained, updating the geometry of the model, the analysis is called two-way coupling. On the other hand, if the fire modelling is performed for the entire interval of interest without updating the geometry, the analysis is called one-way coupling. It is evident that a two-way coupling analysis is more accurate; however, its computational cost is considerably higher. For this reason, and despite the loss of precision, the one-way coupling is generally chosen. One-way coupling is ideal when structural deformations are small and do not significantly alter the fire flow field. On the other hand, for complex phenomena such as progressive collapse, coating detachment, or significant geometric changes, bidirectional coupling is necessary (see [1–4,11,12]).

2.1. CFD-FEM Model

This work will use a one-way coupling model to evaluate a localized fire in an RCB. The study employs a model created in the open-source tool Fire Dynamics Simulator - FDS to represent the fire scenario. This software has been widely validated by various institutions and offers a practical option for this type of study. The FDS relies on CFD techniques for its simulations, being able to obtain convection coefficients, heat flows, and gas temperatures, among others, in the domain considered at the time of interest. To guarantee convergence of the results, it is necessary that the relationship between the characteristic length of the hexahedral cell of the model mesh and the characteristic fire diameter [17], calculated according to Equation (2), is at least 16.

$$D^{*}=\left(\frac{HRR}{\rho_{\infty}c_{p}\theta_{\infty}\sqrt{g}}\right)^{2/5} \quad (2)$$

Where HRR represents the rate of heat release, c_p denotes the specific heat coefficient at constant air pressure, θ_∞ represents the ambient air temperature, ρ_∞ Stands for the air density, and g corresponds to the gravitational acceleration.

FDS solves Equation (1) through the use of the Adiabatic Surface Temperature approach - θ_{AST} [K], proposed by [18-21]. This methodology suggests a conceptual substitution in which the boundary subjected to heating is represented by an equivalent surface with idealized thermal insulation properties. Based on this hypothesis, and after doing the appropriate mathematical manipulation, Equation 1 can be rewritten as:

$$q''_{tot}=\varepsilon_s\sigma[(\theta_{AST})^4-(\theta_s)^4]+h_c(\theta_{AST}-\theta_s) \quad (3)$$

The values of θ_{AST} and h_c are recorded over time by means of sensors implemented on the affected surface of the structure. These values allow calculating the heat fluxes to estimate the temperature field. Despite the advantages in fire analysis in the FDS, it is not common to use it for thermal analysis since it hardly has a 1D heat transfer analysis model implemented. For this reason, the ABAQUS ® software [22] is used in this work, being necessary to use an interface programmed in FORTRAN.

2.2. LF-ESF Model

This modelling approach is extensively described in the previous study, describing and justifying the updates applied to the classical models widely used in the literature. Convection heat flux is evaluated using the ABAQUS subroutine DFLUX, which allows for a value of h_c and the temperature field to be considered at each position. In this analysis, a single value of h_c (15 $[\frac{W}{m^2-K}]$), was considered, as recommended by the EN 1991-1-2 standard [3]. The temperature distribution $\theta_{(z)}$ $[^oC]$ is described by equation (4):

$$\theta_{(z)}=\frac{0.3785}{\bar{H}_{fl}}-\frac{0.02}{\bar{H}_{fl}}\bar{r}+0.57\cdot e^{1.3\bar{H}_{fl}(1-\bar{r})} \quad (4)$$

Where $\bar{H}_{fl}=\frac{H_{fl}}{z}[m]$ refers to the normalized height, $H_{fl}\,[m]$ denotes the flame's height; $\bar{r}=r/(D/2)\,[m]$ corresponds to the distance from the flame axis, expressed in normalized form; $z\,[m]$ represents the elevation at which the temperature is measured. If $\bar{H}_{fl}<1$, considers $\bar{H}_{fl}=1$ in Equation 4.

Radiative heat transfer is modelled using a solid flame whose shape changes from cylindrical to ellipsoidal, as shown in Figure 2. The flame domain is represented by 1896 DS4-type elements arranged uniformly across 79 rows, with a top row composed of 24 DS3-type elements, as illustrated schematically in Figure 4(b). Using the ABAQUS subroutine UMOTION, the flame height can be updated based on the HRR value. This allows the evaluation of the values of the radiation shading factors in the region connecting the structure and the flame front over time. The LF-ESF model also simulates the radiation shadowing effect, which is generally ignored in other simple localized fire models.

2.3. Thermal Analysis

Thermal analysis must solve the governing equation of the heat transfer process, determined by the law of Fourier, shown in Equation 5:

$$\rho c\frac{\partial\theta}{\partial t}=\frac{\partial}{\partial x}\left(k\frac{\partial\theta}{\partial x}\right)+\frac{\partial}{\partial y}\left(k\frac{\partial\theta}{\partial y}\right)+\frac{\partial}{\partial z}\left(k\frac{\partial\theta}{\partial z}\right) \quad (5)$$

Where ρ refers to the density, c represents the specific heat, and k represents the thermal conductivity of concrete or steel, as appropriate. The thermal characteristics of the materials depend on the temperature, as recommended in [1, 2].

To solve Equation 5 using the finite element method, it is necessary to write it in its matrix form, obtaining:

$$[C]\left\{\frac{\partial\theta}{\partial t}\right\}+[K_T]\{\theta\}=\{R_T\} \quad (6)$$

Where [C] denotes the capacitance matrix, $[K_T]$ is the sum of the conductivity matrices ($[K_T]=[K]+[H]$), $\{R_T\}$ is the convection-induced nodal flux vector.

Additionally, Equation 3 must be linearized to be able to use it as a boundary condition since it is not possible to solve a system of fourth-order equations.

$$q''_{tot}=(h_r+h_c)(\theta_{AST}-\theta_s)=h_{tot}^{AST}(\theta_{AST}-\theta_s) \quad (7)$$

Where $h_r=\varepsilon_s\sigma\left[\theta_{AST}{}^2+\theta_s{}^2\right][\theta_{AST}+\theta_s]$ and h_{tot}^{AST} are the adiabatic heat transfer coefficients of radiation and total,

respectively. The temperature field is obtained by applying the scheme shown in Equation 8.

$$\left(\frac{1}{\Delta t}[C]+\beta[K_T]\right)\{\theta_s\}_{n+1}=\left(\frac{1}{\Delta t}[C]-(1-\beta)[K_T]\right)\{\theta_s\}_n+(1-\beta)\{R_T\}_n+\beta\{R_T\}_{n+1} \quad (8)$$

Where Δt is the time step, and β represents the coefficient with temporal integration.

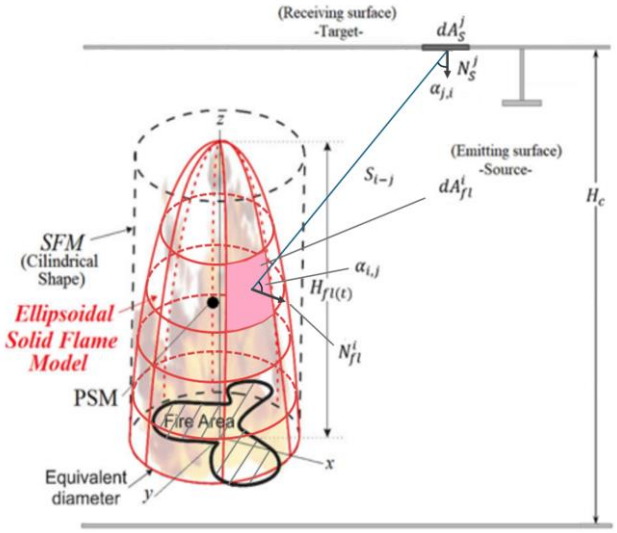

Fig. 2. Heat transfer by radiation occurring between two infinitesimal surface areas

3. Case Study

The purpose of this research is to show the necessary steps for the analysis of RCB in localized fire scenarios. For this purpose, a fire simulation is performed using a model in FDS version 6.2 [23, 24] and the LF-ESF model. Once this simulation is completed, the estimated heat fluxes are introduced into a finite element thermal model (in this work, developed in Abaqus® software [22]), in order to calculate the temperature field resulting from this specific fire scenario.

Considering the widespread use of these beams in diverse structural applications, the typical rectangular section (0.5×0.4 m) beam shown in Figure 3 is selected. The reinforcing bars and stirrups measure 24 mm and 16 mm in diameter, respectively. The RCB has a length of 3 m, and its bottom is positioned 2.5 m above ground level. The fire scenario considers the burning of propane in a 1 m diameter well situated on the floor in the mid-position of the beam length.

The fire scenario assumes a Heat Release Rate – HRR curve with a constant value of 800 kW. The said curve has a 2-minute parabolic growth stage of the fire, followed by a constant regime that lasts about 27 minutes, and then decays linearly during the last 16 minutes of the considered fire scenario.

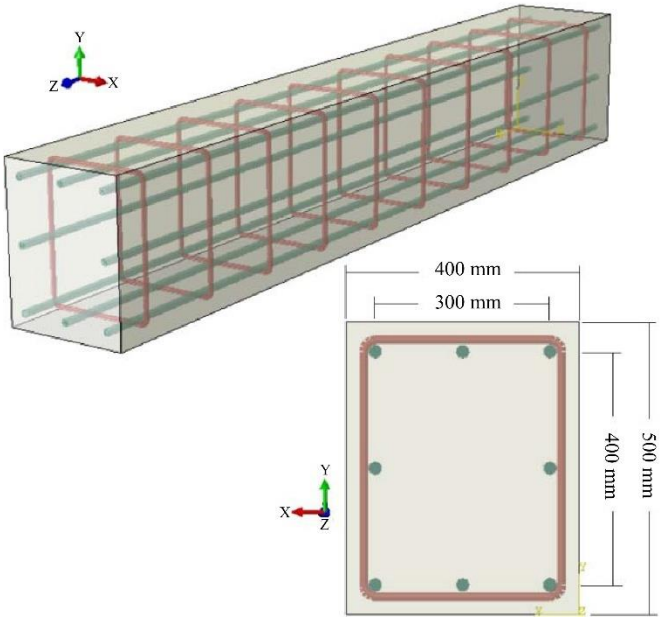

Fig. 3 Schematic representation and main dimensions of the analysed Reinforced Concrete Beam

Figure 4 depicts the FDS configuration, which considers a width of 4 m, with a height and depth of 3 m. This model consists of 72x54x54 hexahedral elements, equivalent to 209952 elements. On the exposed surface of the RCB, a series of virtual sensors were placed that are capable of capturing and storing the values of θ_{AST} and h_{tot}^{AST}, throughout the analysis time. For thermal evaluation, a numerical model based on the finite element method was implemented in ABAQUS [22]. This program change is due to the fact that the FDS considers a linear (1D) model for heat transfer analysis, while the EF model considers a 3D model. The thermal model only considers the modelling of the beam that is discretized using 4x5x30 hexahedral elements of the DC3D8 type for the concrete beam. The coupling of information between FDS and FEM, with a fine mesh in FDS to a coarser mesh in FEM, is performed by a spatial and temporal interpolation process, where each FEM surface receives the average or interpolated value of the corresponding FDS cells. The reinforcement bar and stirrup are modelled using elements of the DC1D2 wire type. The bar and the stirrup are modelled using the technique of embedded elements within the concrete column, that is, only the centroidal axes are considered, informing the program of the thermal properties, according to the temperature, the steel characteristics, and the cross-sectional area. The program automatically performs the removal of concrete material and the connection between concrete and steel for all practical purposes. This technique allows us to avoid the tedious modelling of the bars and stirrups and the necessary removal of the concrete in the volume that they occupy. Once the values of θ_{AST} and h_{tot}^{AST} have been processed, they are entered into the exposed surfaces of the corresponding elements, and the program performs the calculation of the thermal field in approximately 2 minutes.

This methodology was validated in the authors' publication [20], where a full-scale experiment carried out in Sweden was reproduced.

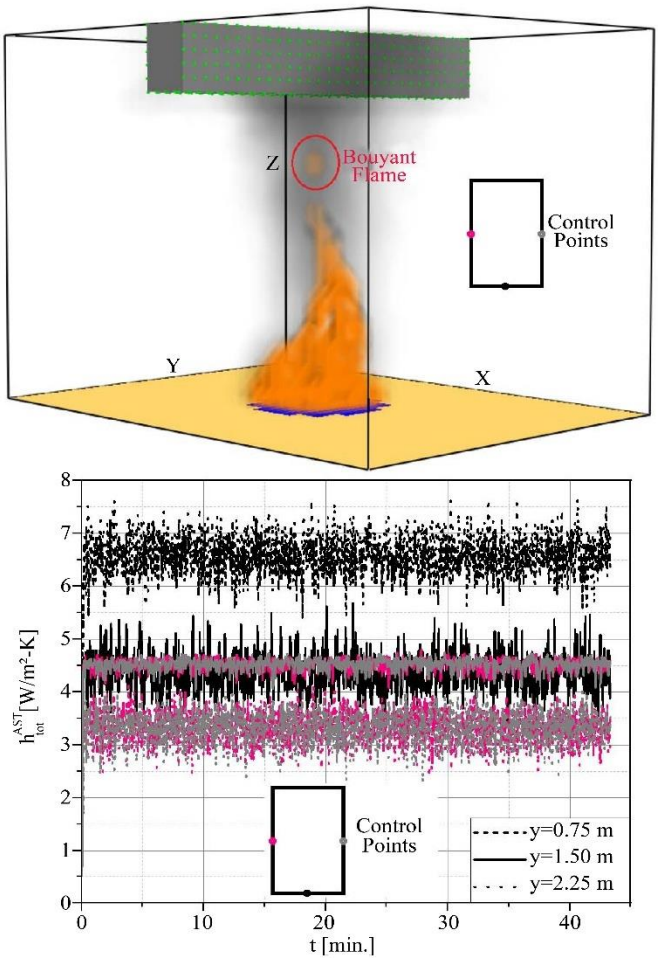

Fig. 4 (a) Buoyant flame and hot gases in the FDS model for $t = 12$ minutes, and (b) Temporal distribution of the heat transfer coefficients at control points.

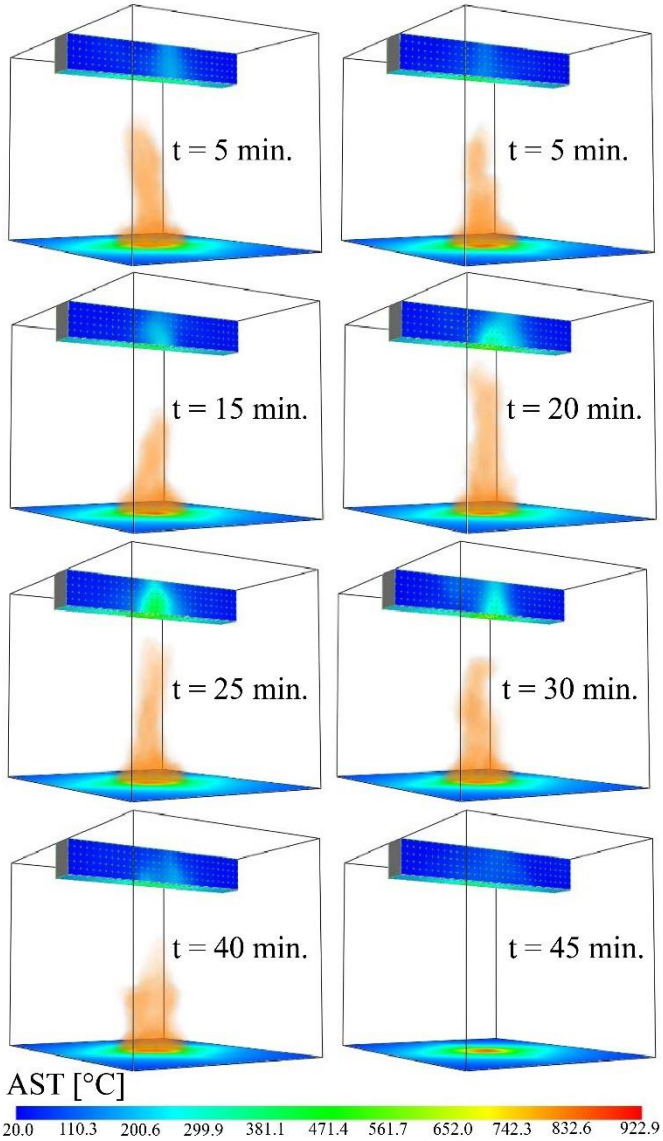

Fig. 5 Adiabatic surface temperature fields and flame's shape for different time instants

4. Results and Discussion

4.1. Fire Simulation

Figure 4(a) displays, at t=12 minutes, the shape of the flame, the distribution of hot gases, and Figure 4(b) shows the distribution of heat transfer coefficients for the points located at y=0.75m,1.5 m, and 2.25 m as shown in the diagram. The flame, in general, is composed of a constant region, an intermittent region, and a fluctuating region. Note that the first one generally maintains the height and shape, while the intermittent region is generated due to the pressure changes that occur when solving the fluid dynamics problem. The fluctuating region is due to small detachments of parts of the flame due to the density differences that occur due to the mentioned pressure changes. Although the case study considers the upper open surface as a boundary condition, allowing the escape of hot gases, these can reduce the intensity of thermal radiation incident on the beam surface.

Regarding the total heat transfer coefficients h_{tot}^{AST} in Figure 4(b), it is observed that in the middle region of the beam ($y = 1.5$ m), the average value is 4.5 [kW/m2-K] while in the extremes in the lower region, its average value is 7.25 [kW/m2-K] and in the sides at both ends, its average value is 3.3 [kW/m2-K].

Figure 5 shows the temperature field θ_{AST} for different time instants as well as the flame's shape. To enhance the representation of this thermal field, the distribution of the hot gases is not shown. The maximum temperatures are found in the region where the pool is located, as can be seen at the 45-minute instant, when the flame was extinguished. In the beam, as expected, the maximum temperatures are found in the region directly above the flame, in which temperatures of the order of θ_{AST}=420 [ºC] are reached.

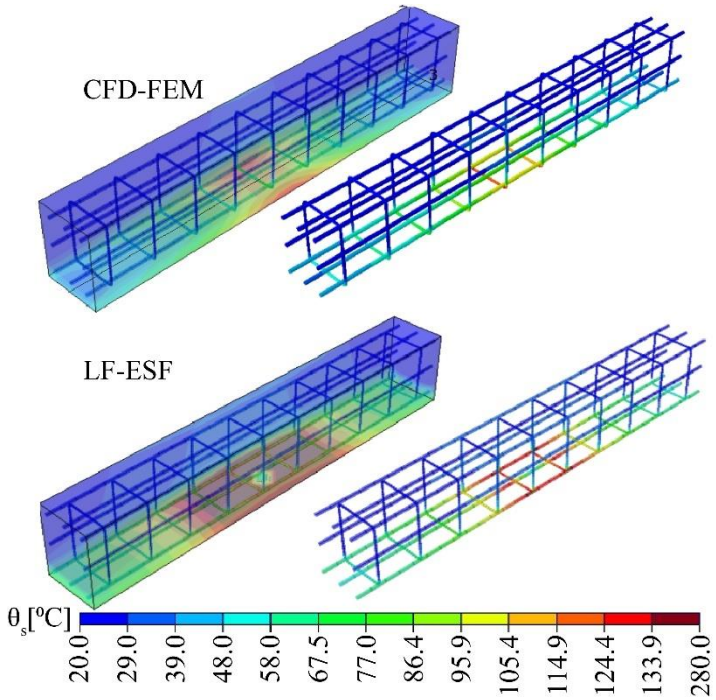

Fig. 6 Temperature field in the beam and reinforcements (embedded elements) at the instant of maximum temperature ($t = 30$ minutes)

In relation to the flame, it can be seen that despite the fact that most of the moments presented are within the region of stable behaviour of the HRR, the shape is not constant. The flame barely represents the visible part of the fuel-burning process, and its shape, height, and inclination are strongly influenced by the boundary conditions, among which are the openings in the behaviour (which affect the distribution of pressure inside it), wind speed, among others.

4.2. Thermal Analysis

Once the simulation of the fire by the FDS model has been completed, the values of θ_{AST} and h_c, captured by the virtual sensors, are processed and subsequently introduced into the finite element thermal model. The fire scenario, described in item 3, is calculated in approximately 2 minutes. Figure 6 shows, for the moment when the peak temperature occurs (approximately at $t = 30$ minutes), the temperature field in the beam and its reinforcing elements. As expected, the region directly above the flame in the lower part presents the highest temperatures, concentrating on the edges because in this region, the hot gases interact with the beam's bottom and sides; therefore, the predominant process is convective heat transfer. The reinforcement elements are shown rendered, that is, their actual surface is shown, and not only their centroidal axis, since they were modelled with the embedded element technique. In the case of the CFD-FEM model, a maximum temperature of 133.9 °C is observed, while the LF-ESF model presents maximum temperatures of around 280 °C. The differences, although significant, are because in the CFD-FEM model, the flame shape is constantly updated, whereas within the LF-ESF model, the shape is constant in the region of constant HRR behaviour.

Figure 7 illustrates the temperature distribution in the concrete for cross sections located at $z = 0.5,\ 1.0,$ and $1.5\ m$ for different moments of time. The light blue dots represent the location of the reinforcing bars. The temperature distribution in the lower region shows that the radiation heat transfer process is predominant in this region despite being partially blocked by the flue gases. At $z = 0.5$, the almost uniform temperature increases in the lower part of the beam can be seen, unlike the other sections, because the hot gases escape into the environment, and there is no convective heat transfer process in this region. In the centre of the beam ($z = 1.5\ m$), the presence of hot gases generates perceptible temperature increases in the lateral regions of the beam.

For $z = 1.5\ m$ at $t = 30$ minutes, the concentration of the highest temperatures in the lower corners of the beam becomes evident, since the presence of hot gases near the sides enhances the convective heat transfer in this region. If the boundary conditions were different, for example, in the presence of a roof, this would block the free flux of hot gases, modifying the temperature profile obtained. In the same way, if the analysis were carried out with a simple model such as the ISO-834 fire curve [2, 25, 26], where the same temperature is considered on the 3 exposed faces of the beam, the results would be significantly different. The differences between the temperatures obtained by each of the models are shown most significantly in the lower region of the beam.

Figure 8 presents the time-dependent temperature variation at different monitoring points within the concrete beam, the stirrups, and the steel bars, respectively, for the section located at z=1.5 m. In the case of the concrete beam,

the evolution of the four control points is shown, indicating that the maximum temperature occurs approximately 30 minutes after the start, followed by a cooling process. In the case of the stirrups, four control points are also shown, making it evident that the maximum temperatures occur at a later time, caused by the retardation of the heat flow process between the concrete and the stirrups. Finally, for the bar in the lower corner, the peak temperature is reached after about 35 minutes.

For the other bars, there is a delay in reaching their maximum temperature due to the influence of their position and the delay in the heat propagation process between the steel and the concrete. In this case, the continuous curves obtained by the CFD-FEM model are smooth, while the dashed curves, which correspond to the LF-ESF model, show an inflection point around 30 minutes after the fire. This is where the maximum values are obtained for this model.

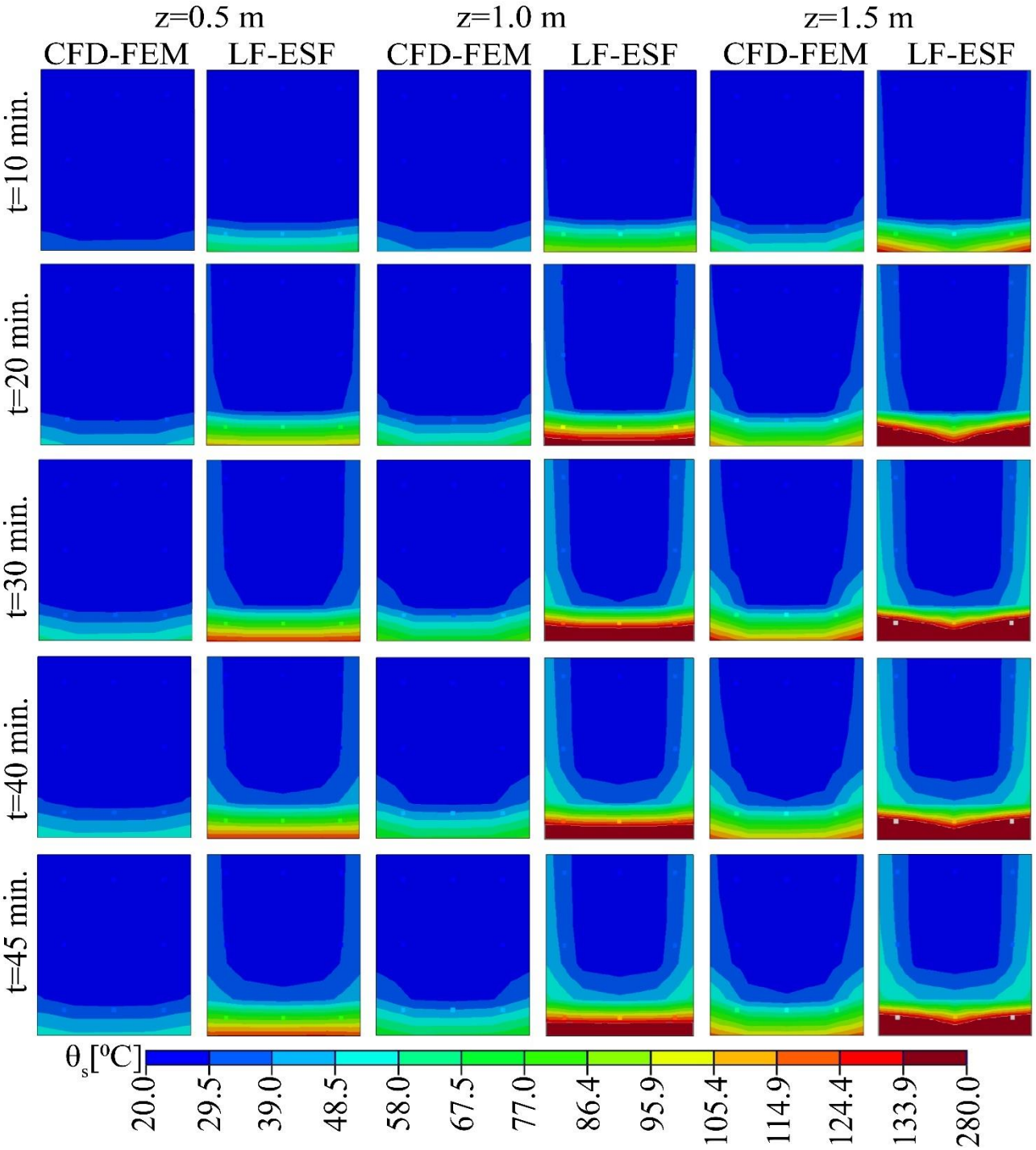

Fig. 7 Temperature field for different RCB sections

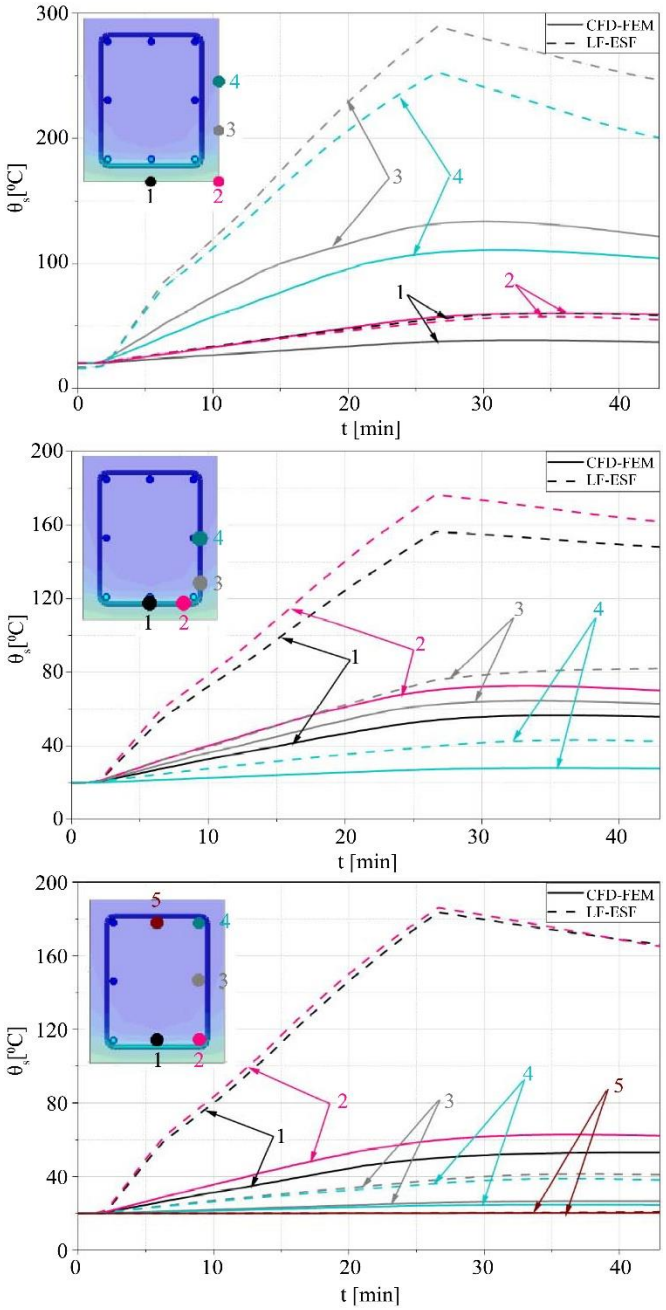

Fig. 8 Temperature variation at monitoring points across the RCB cross section at $z = 1.5\ m$.

5. Conclusion

From the findings of the case study, it can be stated that the use of CFD-FEM and LF-ESF models for assessing the thermal behaviour of RC structures in localized fire situations consistently and qualitatively represents the phenomenon studied. The LF-ESF model presents conservative results, but it has in its favour the easy implementation necessary for this type of analysis. The results show that the RCB region above the flame presents a radiation heat transfer process, despite being partially blocked by the combustion gases. However, the convective heat transfer process predominates due to the interaction of hot gases; as a result, the beam's bottom corners exhibit the highest temperatures. The maximum temperature in the stirrups and bars in the centre of the beam occurs with a delay of 2.5 and 5 minutes, respectively, with respect to the moment at which the concrete reaches the maximum temperature. As expected, the cooling process is slower in the bars and stirrups.

The need to use materials with different thermal properties, as well as the use of materials embedded in others to facilitate the implementation of the model to be studied, increases the complexity of the study. The high conductivity of steel generates thermal gradients that are difficult to reproduce numerically. This necessitates the use of refined computational meshes to adequately capture these gradients. The computational power required, as well as the time required to complete it, increases considerably. Despite the limitation of the study to the thermal part, it is necessary to understand that the more accurate the depiction of the temperature field, the better the evaluation of the thermomechanical behaviour of the structure. This type of analysis, in general, is limited to the evaluation of real accidents, opting for simple methodologies for the analysis of fire conditions considered during the design process of the structures. It can be concluded that the proposal of this article serves to be applied in different situations and risk analysis in costly undertakings, and to regulate structural parameters. Future work will analyse fire protection in RCB, subject to simple fire models.

Acknowledgments

The author acknowledges the support from Universidad Tecnológica del Perú.

References

[1] EN 1992-1-2: Eurocode 2: Design of Concrete Structures - Part 1-2: General Rules - Structural Fire Design, 1992. [Online]. Available: https://www.phd.eng.br/wp-content/uploads/2015/12/en.1992.1.2.2004.pdf

[2] EN 1993-1-2: Eurocode 3: Design of Steel Structures - Part 1-2: General Rules - Structural Fire Design, European Union, 2005. [Online]. Available: https://www.phd.eng.br/wp-content/uploads/2015/12/en.1993.1.2.2005.pdf

[3] EN 1991-1-2: Eurocode 1: Actions on Structures - Part 1-2: General Actions - Actions on Structures Exposed to Fire, European Union, 2002. [Online]. Available: https://www.phd.eng.br/wp-content/uploads/2015/12/en.1991.1.2.2002.pdf

[4] Morgan J. Hurley et al., *SFPE Handbook of Fire Protection Engineering*, 5th ed., Springer Nature, 2016. [CrossRef] [Google Scholar] [Publisher Link]

[5] Jose Alos-Moya et al., "Valencia Bridge Fire Tests: Experimental Study of a Composite Bridge under Fire," *Journal of Constructional Steel Research*, vol. 138, pp. 538-554, 2017. [CrossRef] [Google Scholar] [Publisher Link]

[6] Thomaz Eduardo Teixeira Buttignol, "Analytical and Numerical Analyses of RC Beams Exposed to Fire Adopting a LITS Trilinear Constitutive Law for Concrete," *Case Studies in Construction Materials*, vol. 17, pp. 1-20, 2022. [CrossRef] [Google Scholar] [Publisher Link]

[7] Yamin Song et al., "Fire Resistance Investigation of Simple Supported RC Beams with Varying Reinforcement Configurations," *Advances in Civil Engineering*, vol. 2019, no. 1, pp. 1-10, 2019. [CrossRef] [Google Scholar] [Publisher Link]

[8] Aneesha Balaji et al., "Studies on the Behavior of Reinforced Concrete Short Column Subjected to Fire," *Alexandria Engineering Journal*, vol. 55, no. 1, pp. 475-486, 2016. [CrossRef] [Google Scholar] [Publisher Link]

[9] Jinggang Zhou et al., "Comparison of Different CFD-FEM Coupling Methods in Advanced Structural Fire Analysis," *International Journal of Thermal Sciences*, vol. 193, pp. 1-38, 2023. [CrossRef] [Google Scholar] [Publisher Link]

[10] J.A. Feenstra et al., "Automated Two-Way Coupling of CFD Fire Simulations to Thermomechanical FE Analyses at the Overall Structural Level," *Fire Safety Journal*, vol. 96, pp. 165-175, 2018. [CrossRef] [Google Scholar] [Publisher Link]

[11] Julio Cesar G. Silva, Alexandre Landesmann, and Fernando Luiz B. Ribeiro, "Fire-Thermomechanical Interface Model for Performance-Based Analysis of Structures Exposed to Fire," *Fire Safety Journal*, vol. 83, pp. 66-78, 2016. [CrossRef] [Google Scholar] [Publisher Link]

[12] Chao Zhang et al., "Simulation Methodology for Coupled Fire-Structure Analysis: Modeling Localized Fire Tests on a Steel Column," *Fire Technology*, vol. 52, no. 1, pp. 239-262, 2016. [CrossRef] [Google Scholar] [Publisher Link]

[13] Chao Zhang, Guo-Qiang Li, and Asif Usmani, "Simulating the Behavior of Restrained Steel Beams to Flame Impingement from Localized-Fires," *Journal of Constructional Steel Research*, vol. 83, pp. 156-165, 2013. [CrossRef] [Google Scholar] [Publisher Link]

[14] Min Gyu Ryu et al., "Finite Element Modeling for the Progressive Collapse Analysis of Steel Stiffened-Plate Structures in Fires," *Thin-Walled Structures*, vol. 159, 2021. [CrossRef] [Google Scholar] [Publisher Link]

[15] Qing Xu, Guo-Qiang Li, and Yong C. Wang, "A Simplified Method for Calculating Non-Uniform Temperature Distributions in Thin-Walled Steel Members Protected by Intumescent Coatings under Localized Fires," *Thin-Walled Structures*, vol. 162, 2021. [CrossRef] [Google Scholar] [Publisher Link]

[16] I. Payá-Zaforteza, and M.E.M. Garlock, "A Numerical Investigation on the Fire Response of a Steel Girder Bridge," *Journal of Constructional Steel Research*, vol. 75, pp. 93-103, 2012. [CrossRef] [Google Scholar] [Publisher Link]

[17] Rachel Wasson et al., "Influence of a Ceiling on Fire Plume Velocity and Temperature," *Fire Technology*, vol. 52, no. 6, pp. 1863-1886, 2015. [CrossRef] [Google Scholar] [Publisher Link]

[18] U. Wickström, "The Adiabatic Surface Temperature and the Plate Thermometer," *Fire Safety Science*, pp. 1001-1011, 2011. [CrossRef] [Google Scholar] [Publisher Link]

[19] Ulf Wickström, Johan Anderson, and Johan Sjöström, "Measuring Incident Heat Flux and Adiabatic Surface Temperature with Plate Thermometers in Ambient and High Temperatures," *Fire and Materials*, vol. 43, no. 1, pp. 51-56, 2019. [CrossRef] [Google Scholar] [Publisher Link]

[20] J. Sjostrom et al., Thermal Exposure to a Steel Column from Localized Fires, Science Partner Technical Research Institute of Swedan, 2012. [Google Scholar] [Publisher Link]

[21] Ulf Wickström et al., "Technical Comment-Ten Fundamental Principles on Defining and Expressing Thermal Exposure as Boundary Conditions in Fire Safety Engineering," *Fire and Materials*, vol. 42, no. 8, pp. 985-988, 2018. [CrossRef] [Google Scholar] [Publisher Link]

[22] Simulia D.S., "Abaqus 6.12 documentation. Providence, Rhode Island, US 2012:6. [Google Scholar] [Publisher Link]

[23] Kevin B. McGrattan et al., Fire Dynamics Simulator-Technical Reference Guide, National Institute of Standards and Technology, 2015. [Online]. Available: https://nvlpubs.nist.gov/nistpubs/Legacy/IR/nistir6467.pdf

[24] Kevin McGrattan et al., *Fire Dynamics Simulator, User's Guide*, National Institute of Standards and Technology Engineering Laboratory, 6th ed., 2015. [Google Scholar]

[25] James G. Quintiere, *Fundamentals of Fire Phenomena*, 2006. [CrossRef] [Google Scholar] [Publisher Link]

[26] Chao Zhang, Zhe Zhang, and Guo-Qiang Li, "Simple vs. Sophisticated Fire Models to Predict Performance of SHS Column in Localized Fire," *Journal of Constructional Steel Research*, vol. 120, pp. 62-69, 2016. [CrossRef] [Google Scholar] [Publisher Link]